Wiley Online Library
Early View publication on www.wileyonlinelibrary.com
(issue and page numbers not yet assigned;
citable using Digital Object Identifier – DOI)

J. Biophotonics 1–9 (2016) / **DOI** 10.1002/jbio.201600132

Journal of BIOPHOTONICS

FULL ARTICLE

Intravital excitation increases detection sensitivity for pulmonary tuberculosis by whole-body imaging with β-lactamase reporter enzyme fluorescence

Fatemeh Nooshabadi[**,1], *Hee-Jeong Yang*[**,2], *Yunfeng Cheng*[**,3], *Madeleine S. Durkee*[1], *Hexin Xie*[3], *Jianghong Rao*[3], *Jeffrey D. Cirillo*[2], *and Kristen C. Maitland*[*,1]

[1] Biomedical Engineering Department, 3120 TAMU, Texas A&M University, College Station, TX 77843, United States
[2] Microbial Pathogenesis and Immunology Department, Texas A&M University Health Science Center, Bryan, Texas, 77807, United States
[3] Radiology Department, Stanford University, Stanford, CA 94304, United States

Received 29 April 2016, revised 8 August 2016, accepted 18 September 2016
Published online 19 October 2016

Key words: intravital microscopy, *in vivo* imaging, tuberculosis, fluorescence, whole-animal imaging

Tuberculosis is a pulmonary disease with an especially high mortality rate in immuno-compromised populations, specifically children and HIV positive individuals. The causative agent, *Mycobacterium tuberculosis* (*Mtb*), is a very slow growing and difficult organism to work with, making both diagnosis and development of effective treatments cumbersome. We utilize a fiber-optic fluorescence microendoscope integrated with a whole-body imaging system for *in vivo Mtb* detection. The system exploits an endogenous enzyme of *Mtb* (β-lactamase, or BlaC) using a BlaC-specific NIR fluorogenic substrate. In the presence of BlaC, this substrate is cleaved and becomes fluorescent. Using intravital illumination of the lung to excite this probe, sensitivity of the optical system increases over trans- and epi-illumination methods of whole-body fluorescence imaging. We demonstrate that integration of these imaging technologies with BlaC-specific fluorescent reporter probe improves the level of detection to ~100 colony forming units, a 100× increase in sensitivity in comparison to epi-illumination and a 10× increase in sensitivity in comparison to previous work in intravital excitation of tdTomato-expressing *Mtb*. This lower detection threshold enables the study of early stage bacterial infections with clinical strains of *Mtb* and longitudinal studies of disease pathogenesis and therapeutic efficacy with multiple time points in a single animal.

1. Introduction

Tuberculosis (TB) remains one of the world's deadliest diseases, resulting in an estimated 1.5 million deaths in 2014 [1]. While a staggering one-third of the world's population is infected with *Mycobacterium tuberculosis* (*Mtb*), only 5–15% of these cases develop into active TB. TB is also the leading cause

* Corresponding author: e-mail: kmaitland@tamu.edu
** These authors contributed equally to this work.

of death among people living with human immunodeficiency virus (HIV), contributing to over 30% of deaths of HIV-positive individuals [2]. HIV-positive individuals infected with *Mtb* are 26 times more likely to develop TB than their HIV-negative counterparts. However, for the first time since 2000, the 1.1 million TB deaths in HIV-negative people is approaching and expected to surpass the *total* 1.2 million HIV deaths [2]. Treatment success rates for new TB cases are as high as 85%; however, multidrug-resistant TB (MDR-TB) cases have significantly lower treatment success rates. There is an urgent need to study the mechanisms of *Mtb* pathogenesis, as well as to develop an effective vaccine for disease prevention and new antimycobacterial therapeutic agents to combat MDR-TB.

Whole-body optical imaging of small animals provides non-invasive real-time detection and quantification of *Mtb* bacterial load [3–5]. The standard method of quantification requires sacrifice of animals, tissue homogenization of the organ(s) of interest, plating dilutions on agar plates, and counting of colony-forming units (CFU) after 1–2 months of culture. Recombinant strains of luminescent mycobacteria or fluorescent dye substrates targeted to mycobacteria enables infection monitoring in individual animals over time, reduces the number of animals needed for longitudinal studies, and provides rapid feedback on bacterial load.

We recently demonstrated that intravital fiber-optic excitation in whole-body fluorescence imaging can enhance sensitivity to bacterial load [6]. A fiber bundle microendoscope with illumination centered at 530 nm was integrated into a whole-body imaging system (PerkinElmer; IVIS Lumina II) to facilitate excitation of fluorescence from within the airway, circumventing much of the tissue absorption of excitation light that occurs in conventional epi-illumination. Fluorescence exiting the body was detected via whole-body imaging. The detection threshold for pulmonary infection of tdTomato-expressing *Mycobacterium bovis* BCG (Bacillus Calmette-Guerin) was reduced to $\sim 10^3$ CFU by incorporating intravital excitation [6]. In comparison, fluorescence detected with whole-body epi-illumination of mice infected with up to 10^6 CFU tdTomato-expressing BCG was not significantly different than autofluorescence signal detected in pulmonary infections of BCG with vector backbone. Although recombinant reporter strains of mycobacteria have been widely used for *in vivo* imaging, these techniques require specific recombinant laboratory strains that are not present in clinical samples [7–14]. Preclinical evaluation of new vaccines would be best performed using both laboratory and clinical *Mtb* isolates to improve predictive value of animal studies for human efficacy [15]. Furthermore, optical technologies targeted to clinical strains, rather than recombinant strains, have the potential for clinical translation as either *in vitro* or *in vivo* rapid point-of-care diagnostic tools [16].

We have developed reporter enzyme fluorescence (REF) technology to detect tuberculosis in live animals without recombinant strains that can facilitate the clinical need for improved TB detection tools [17]. The REF system uses a custom fluorogenic substrate designed to be cleaved by the bacterial enzyme BlaC, which is naturally endogenously expressed in *Mtb* and belongs to the class A β-lactamase family [16]. Although β-lactamase enzymes are present on many mycobacteria, BlaC is specific to virulent *Mtb* strains [18]. Moreover, previous studies reported that BlaC expression was constitutive both in active and latent TB, indicating that the REF system allows detection of any phase of TB [19]. One of the main advantages of REF is that no recombinant strain is needed, enabling clinical translation of the technology. The REF system uses a near-infrared (NIR) fluorescent dye in a custom fluorogenic substrate, which is more suitable for *in vivo* imaging due to the longer tissue penetration and lower autofluorescence background of NIR light [20–23]. REF imaging using BlaC-specific NIR substrate has made a significant breakthrough in whole animal imaging of tuberculosis [3, 16, 17]. The REF substrate CNIR800 has recently been developed for sensitive and specific detection of tuberculosis in live animals [24]. CNIR800 carries the NIR fluorophore IRDye 800CW, which has been used in human cells and tissues *in situ* and *in vivo*, particularly for application to cancer imaging and monitoring of therapy [25–29]. This progress supports potential future translation of CNIR800 for clinical applications in tuberculosis. In this study, we exploit intravital excitation via a microendoscope to improve sensitivity of whole-body imaging to detect REF substrate cleaved by mycobacteria-expressed β-lactamase in the mouse lung. The improved sensitivity gained by intravital excitation is necessary for diagnosis of early stage TB infections and to evaluate therapeutic outcomes in animal models.

2. Methods

2.1 Animal infections

Mice were randomly grouped in six groups of four mice per group. The mice were anesthetized and infected with 10–10^6 CFU of *M. bovis* BCG strain by intratracheal instillation. *M. bovis* BCG strain was used in this study as a safety precaution because it is closely related to *M. tuberculosis* but not virulent in humans [30]. A detailed protocol for the method of infection was described previously [31]. 24 hours after inoculation, the mice were imaged using the

whole-body imaging system with intravital excitation. Following imaging, the lungs were excised, homogenized, and 10-fold serial dilutions of lung homogenates were plated on 7H11 selective media for culturing and CFU counting.

Animal use protocols were approved by the Texas A&M University Institutional Animal Care and Use Committee. Five- to seven-week old female BALB/C mice were used in this study. Mice were fed alfalfa-free AIN-93G diet with *ad libitum* access to water. A mixture of ketamine (100 mg/kg) and xylazine (10 mg/kg) was used for anesthesia.

2.2 Reporter enzyme fluorescence technology and substrate CNIR800

The CNIR800 substrate consists of IRDye 800CW fluorescent dye linked to a quencher (IRDye QC-1) at the distal end through a lactam ring, providing a fluorescence resonance energy transfer (FRET) quenching effect (Figure 1) [17]. In the absence of BlaC (no mycobacteria), the substrate is quenched and produces minimal fluorescence. BlaC cleavage of the lactam ring releases the quencher from CNIR800, significantly increasing fluorescence of the IRDye. Cleaved CNIR800 displays maximal signal at an emission wavelength of 795 nm with 745 nm peak excitation wavelength [24]. The CNIR800 REF substrate (20 µM, 2.5 µl/g of weight) was administered intratracheally at 24 hours post-infection.

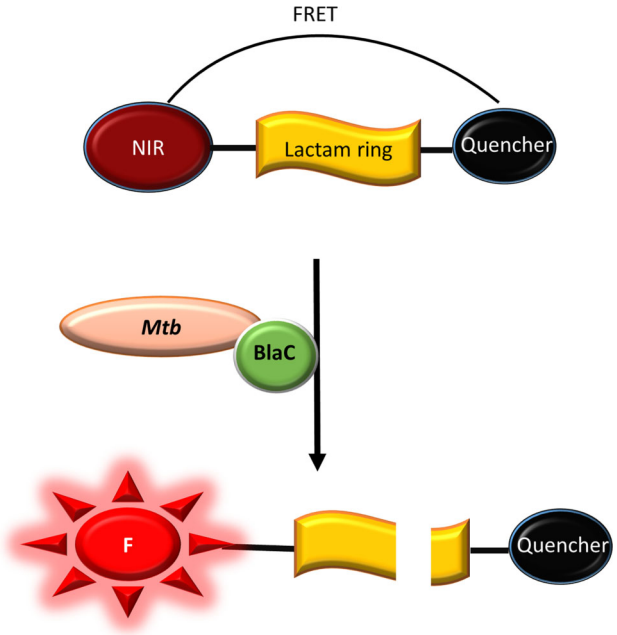

Figure 1 Schematic representation of the reporter enzyme fluorescence (REF) system. The β-lactamase enzyme naturally and constitutively expressed in *Mycobacterium tuberculosis* cleaves the lactam ring in the substrate, releasing the FRET quencher and allowing recovery of IRDye 800CW fluorescence.

2.3 Whole-body fluorescence imaging system with intravital excitation

Figure 2 shows the integrated whole-body imaging system with intravital excitation used in this study,

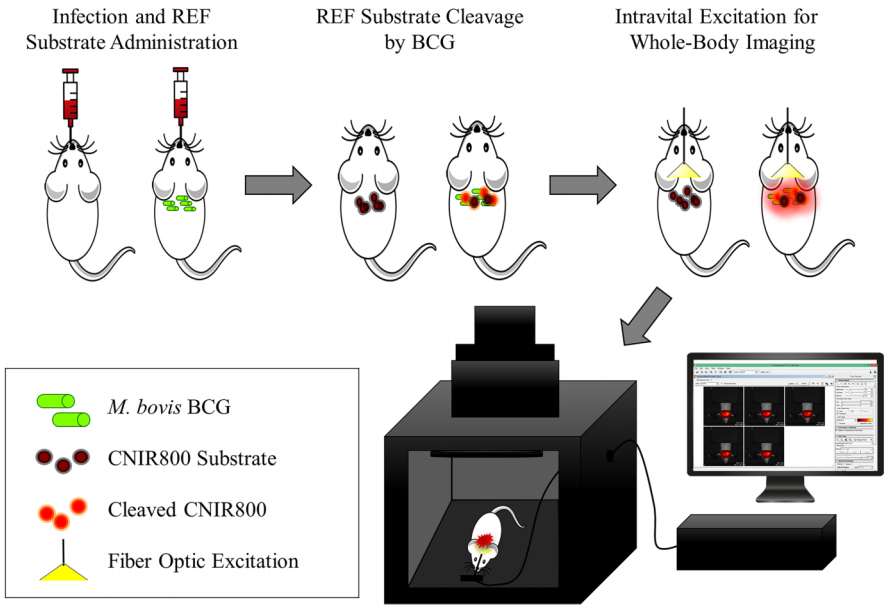

Figure 2 Whole-body imaging of REF fluorescence with intravital excitation in the airway of live mice. 24 hours after BCG infection via intratracheal instillation, CNIR800 REF substrate is administered through an intratracheal catheter. After a time period to allow CNIR800 cleavage, mice are placed in the whole-body imaging system and the microendoscope is inserted into the airway for intravital excitation and whole-body imaging.

previously described in detail [6]. The fiber-based microendoscope image provides real-time feedback for guidance of placement of the fiber bundle tip within the airway. In tandem, the microendoscope excitation within the airway serves as the intravital light source for whole-body imaging with the IVIS illumination blocked.

The 10,000-fiber bundle (FIGH-10-500N, Fujikura) is routed through an access port into the whole-body imaging system (IVIS Lumina II, PerkinElmer), enabling insertion into the trachea of the anesthetized mouse through a $22G \times 1''$ catheter (SURFLO® I.V. SR-OX2225CA, TERUMO Medical). The excitation pathway of the microendoscope consists of a 730 nm laser diode (HL7302MG, Thorlabs), excitation filter with 750 nm cut-off wavelength (FES0750, Thorlabs) to limit any light leakage, and 757 nm dichroic mirror (FF757-Di01, Semrock) targeting fluorescence excitation of the CNIR800 REF probe. A 10× objective lens (RMS10X, Thorlabs) couples the illumination and imaging system to the fiber bundle. A 776 nm emission filter (FF01-776-LP, Semrock) passes CNIR800 fluorescence to a 1.45 megapixel CCD camera (EXi Blue, QImaging). The microendoscope fiber bundle has 0.66 mm outer diameter, 3 μm core-to-core spacing, and 450 μm field of view [32]. Output power from the fiber bundle was measured to be 1.2 mW.

2.4 In vivo animal whole-body imaging using REF technology

Whole-body images of mice were acquired using both intravital fiber excitation and IVIS epi-illumination at various time points post-administration of CNIR800. After whole-body imaging, animals were sacrificed and lung homogenates were plated for CFU counting. To collect images with intravital fiber excitation, a catheter was inserted into the trachea of the animal, and the animal was laid on the IVIS stage in the ventral or dorsal position. The lower torso of the mouse was covered with a black cloth to block background fluorescence of the gastrointestinal tract and kidney. The fiber bundle was fed into the catheter until it was in contact with the airway wall. The fiber position was guided and confirmed with the image on the CCD camera of the microendoscope. The fiber bundle was marked at the mouth to ensure comparable insertion distance among animals and secured to the stage to prevent movement during stage height adjustment for imaging.

The excitation light source from the IVIS system was blocked, and IVIS fluorescence emission filters were selected to collect CNIR800 signal at 20 nm increments from 760 nm to 840 m using the IVIS camera in order to spectrally unmix the image data. After imaging with intravital excitation, epi-illumination images of the same animal with the IVIS imaging system excitation source were collected for comparison. Epi-illumination band-pass excitation filters of 675 nm and 745 nm were used for background tissue autofluorescence and CNIR800, respectively. Typical IVIS illumination intensity was approximately 1–2 $\mu W/cm^2$. The same IVIS emission filter settings were used as the intravital fiber excitation configuration. Each acquisition was taken with an f-stop of 2, medium binning, and automatic exposure time, which maximizes the sensitivity to signal. Acquisition settings are automatically recorded and fluorescence signal is quantified by the software.

Manual spectral unmixing was performed using PerkinElmer Living Image software (version 4.3.1) to reduce tissue autofluorescence background and quantify the REF signal detected by whole-body imaging with intravital or epi-illumination. Following spectral unmixing, fluorescence radiance was quantified over a pre-defined region of interest targeting the lungs.

Statistical analysis was performed using GraphPad Prism software (Version 6). Student's two-tailed *t*-test was used to determine statistical significance compared to the control; $P < 0.05$ was considered significant. Pearson correlation was used to test the correlation of CFU and fluorescence signals. The relationship between CFU and fluorescence signal was determined using a linear regression analysis.

3. Results

3.1 Peak CNIR800 substrate fluorescence signal at 4 hours post-pulmonary administration

At 24 hours post-inoculation, CNIR800 was delivered by aerosol to two mice infected with 10^6 CFU of *M. bovis* BCG strain and two uninfected mice to evaluate the kinetics of the REF substrate CNIR800 to detect bacterial infection in the mouse lung. Pulmonary delivery of substrates improves signal-to-noise ratio (SNR) by concentrating delivery to the target infection site and decreasing background signal from other organs and tissues that could otherwise accumulate substrate. Intravital excitation with whole-body imaging was performed every 2 hours over a 12 hour period (Figure 3A). *In vivo* fluorescence signal from the cleaved substrate significantly increased 2 hours post-administration of the substrate with the maximum fluorescence at 4 hours (Figure 3B). Fluorescence signal in the infected animal at 8 hours post-administration was not significantly different from the initial (0 hours) timepoint,

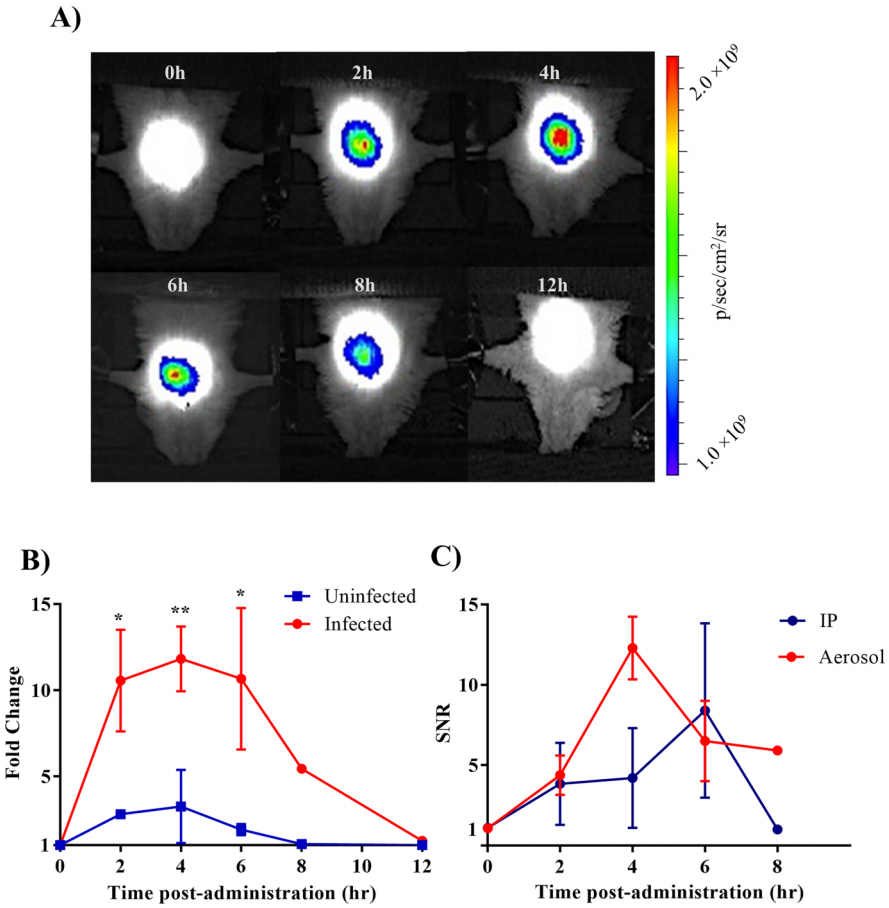

Figure 3 Kinetics of aerosol delivery of CNIR800 (20 µM, 2.5 µl/g) in mice infected with 10^6 CFU *M. bovis* BCG strain in the lungs. (**A**) Whole-body images acquired with intravital excitation at time points post-administration of CNIR800. (**B**) Comparison of mean fluorescence signal fold-change over signal at initial time point for infected and uninfected mice. * p-value < 0.05, ** p-value < 0.01: significantly different from fluorescence signal at 0 hour using Student's two-tailed t-test. (**C**) Comparison of mean signal-to-noise ratio (SNR) fold-change for aerosol delivery and intraperitoneal delivery of CNIR800. Error bars denote standard error.

suggesting that the ideal window for imaging by pulmonary delivery of CNIR800 is between 2 and 6 hours post-administration of the substrate. Aerosol delivery into the airway showed faster kinetics than intraperitoneal (IP) delivery of the substrate, which had a gradual signal increase from 2 hours until it reached a maximum at 6 hours post-administration (Figure 3C).

3.2 Dorsal position exhibits the highest SNR at 4 hours post-administration of CNIR800

Groups of mice infected with 10^6 CFU *M. bovis* BCG strain were imaged at 2 and 4 hours post-administration of CNIR800 substrate in dorsal and ventral positions on the IVIS stage. SNR was calculated at each time point by dividing fluorescence signal detected in infected mice by the signal in uninfected mice for each position (Figure 4C). At 2 hours post-administration, both positions exhibited a similar SNR. However, at 4 hours post-administration, SNR was significantly increased in dorsal position as compared to the ventral position despite the fluorescence signal being higher in the ventral position. The SNR of the images in the dorsal position at 4 hours post-administration was also significantly higher than the same position at 2 hours post-administration ($P = 0.029$).

3.3 Detecting pulmonary infection in mice using BlaC-specific substrate

Six groups of mice were infected with 10^1–10^6 CFU of *M. bovis* BCG intratracheally, and CNIR800 was delivered to the mice via aerosol at 24 hours post-infection. Mice were first imaged using intravital fiber-optic excitation 4 hours post-administration of the substrate. Immediately after, mice were imaged using epi-illumination of whole-body imaging system (IVIS Lumina II) for parallel comparison of these systems. As shown in Figure 5, whole-body imaging with intravital fiber-optic excitation using CNIR800 provided a threshold of detection as low as ~100 CFU in the mouse lung (Figure 5C; $P = 0.029$). Fluorescence signals correlated well with the number of bacteria present in mouse lungs down to this threshold (Figure 5C; $R^2 = 0.95$, $P = 0.0008$), while epi-illumination of the animal only allowed detection

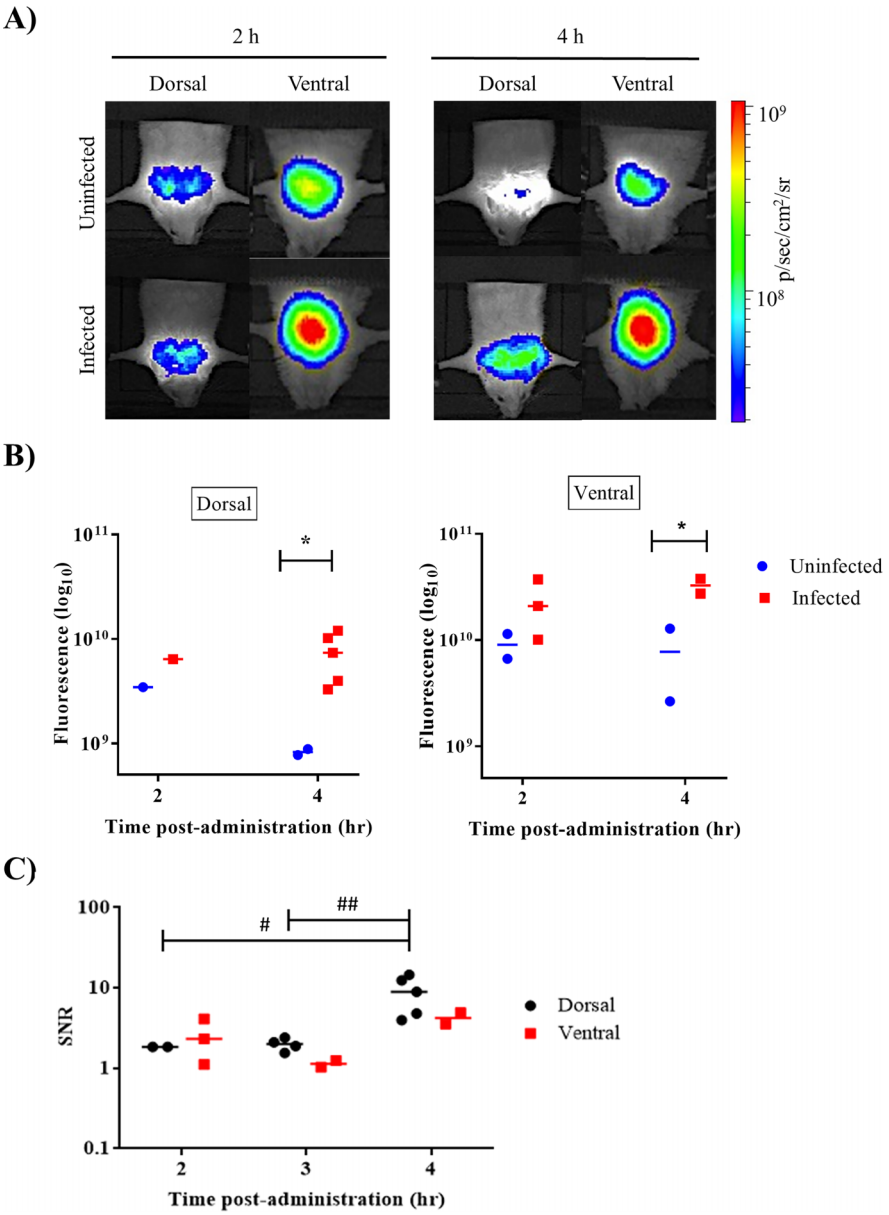

Figure 4 Effect of animal positioning on fluorescence detection and signal-to-noise ratio (SNR) in whole-body imaging with intravital excitation after aerosol delivery of CNIR800 in mice infected with 10^6 CFU *M. bovis* BCG strain in the lungs. (**A**) Representative images of mice in dorsal or ventral position acquired at 2 hours and 4 hours post-administration of CNIR800. Comparison of (**B**) fluorescence signal (photons/sec) and (**C**) SNR (fluorescence signal in infected animals normalized to signal in uninfected animals) in different animal positions at different times post-administration of CNIR800. * p-value < 0.05: significantly different from fluorescence of uninfected control group calculated by Student's t-test; $^{\#}$ p-value < 0.05, $^{\#\#}$ p-value < 0.01: significantly different in fluorescence among different imaging time points calculated by two-way ANOVA.

down to 10^4 CFU (Figure 6C, $R^2 = 0.36$, $P = 0.211$). R^2 was calculated using linear regression. Imaging using intravital fiber-optic excitation therefore improved the threshold of detection over epi-illumination by ~100 fold.

4. Discussion and conclusion

Using a fiber optic fluorescence microendoscope for intravital illumination in a whole-body imaging system, we have characterized the enhancement in signal detection of pulmonary infection *in vivo* using a NIR BlaC-specific fluorogenic substrate in comparison to epi-illumination. We determined optimal methods for achieving the best SNR, including imaging time after fluorogenic substrate administration and the position of the animal during imaging. We demonstrated that integration of these optical imaging technologies with BlaC-specific fluorescent reporter probes enables sensitive detection of bacteria in lungs of living animals at ~100 CFU, an improvement of two orders of magnitude over whole-body epi-illumination. This technology can also improve the sensitivity of whole-body optical imaging to enable study of early stage bacterial infection, evaluation of therapeutic efficacy, and development of preventative treatments using clinical strains of mycobacteria.

The high light scattering ability of lung tissue efficiently diffuses the non-uniform illumination coming

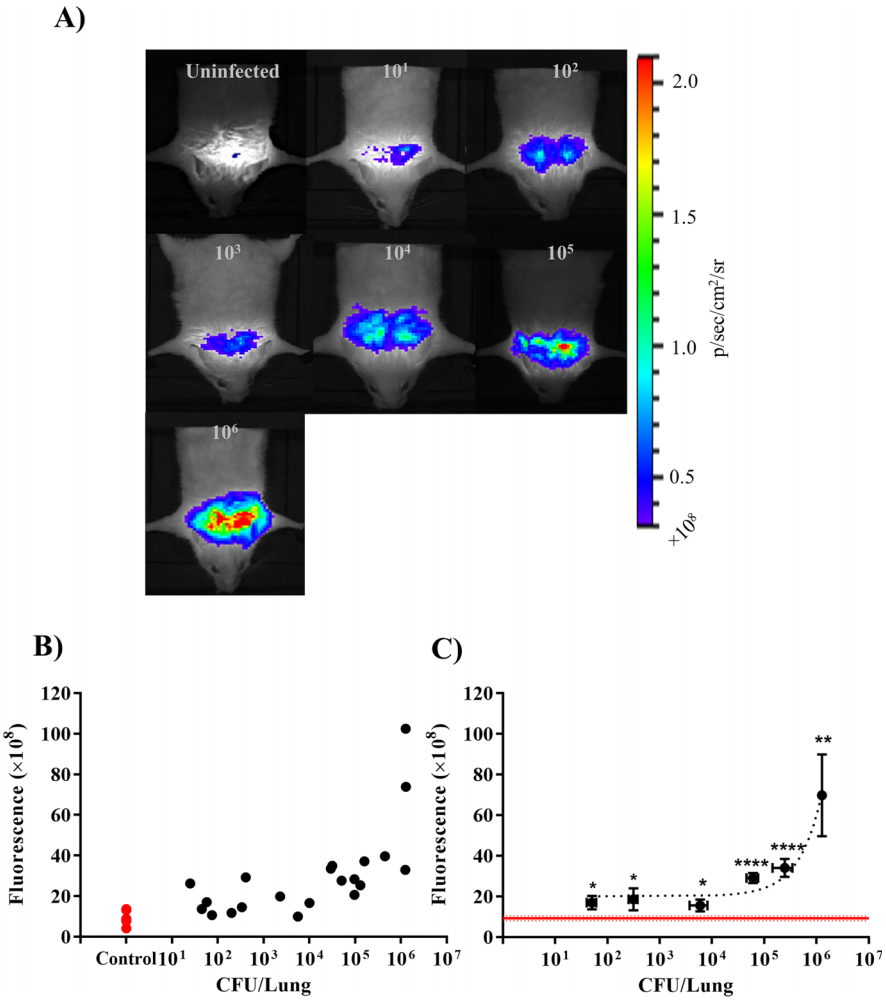

Figure 5 Whole-body imaging using intravital fiber excitation of mice infected with 10–10^6 CFU *M. bovis* BCG strain and labeled with REF substrate CNIR800 delivered intratracheally 24 hours post-infection. (**A**) Representative images 4 hours post-administration of CNIR800. (**B**) Scatter plot of fluorescence signal (photons/sec) for each animal as compared to actual CFU obtained from lung homogenates of same animal. Each dot denotes an individual animal. (**C**) Average fluorescence versus grouped CFU from lung homogenates. Vertical and horizontal error bars represent standard errors of fluorescence and CFU counts per group, respectively. The average fluorescence for the uninfected group is represented by a solid red line; standard error (1.28×10^8 p/sec/cm^2/sr) is represented by dashed red lines that coincide with the mean. * $p < 0.05$, ** $p < 0.01$, *** $p < 0.001$, **** $p < 0.0001$: significantly different as compared to the fluorescence in the uninfected group, calculated by Student's two-tailed *t*-test.

from the fiber bundle source used for intravital illumination. Positioning of the fiber bundle is likely to be important for the quality of imaging obtained. The two primary methods employed to ensure the most repeatable placement of the fiber bundle tip in the mouse airway were consistent insertion of the intratracheal catheter and microendoscopic confirmation of contact with the tissue. Real-time fluorescence images on the microendoscope CCD provide feedback on fiber tip contact with the tissue. Additionally, the fiber bundle was marked at the mouth to confirm positioning of the fiber bundle within mice of the same age and similar weight. In addition to non-uniformity of illumination light distribution, other contributors to fluorescence signal variation likely could include inter-animal variability in distribution of bacterial infection, overall lung volume, and differences in the anatomy of the chest cavity and airways. Epi-illumination images are acquired with longer acquisition times to compensate for lower illumination intensity at the animal compared to intravital illumination intensity. Fluorescence background scales with both illumination intensity and exposure time indicating that level of detection is unaffected.

These results are consistent with our previous report showing significant improvement of detection sensitivity using intravital excitation to detect tdTomato-expressing *M. bovis* BCG in the lungs of live animals [6]. The greater enhancement of intravital excitation over epi-illumination with tdTomato (1000×) in comparison to CNIR800 (100×) can be attributed to the shorter excitation wavelength of tdTomato and higher absorption of shorter wavelengths by mammalian tissue. In other words, intravital excitation is more critical for fluorescent targets with shorter excitation wavelengths. Sources of background in detection of REF substrate are quite different from tdTomato detection. In addition to reduced tissue absorption of NIR light, NIR REF substrates exploit reduced tissue autofluorescence in this spectral range as compared to the visible wavelengths necessary for most genetically modified proteins, including tdTomato. Contributors to background signal for REF detection of mycobacteria include quenched substrate and spontaneous hydro-

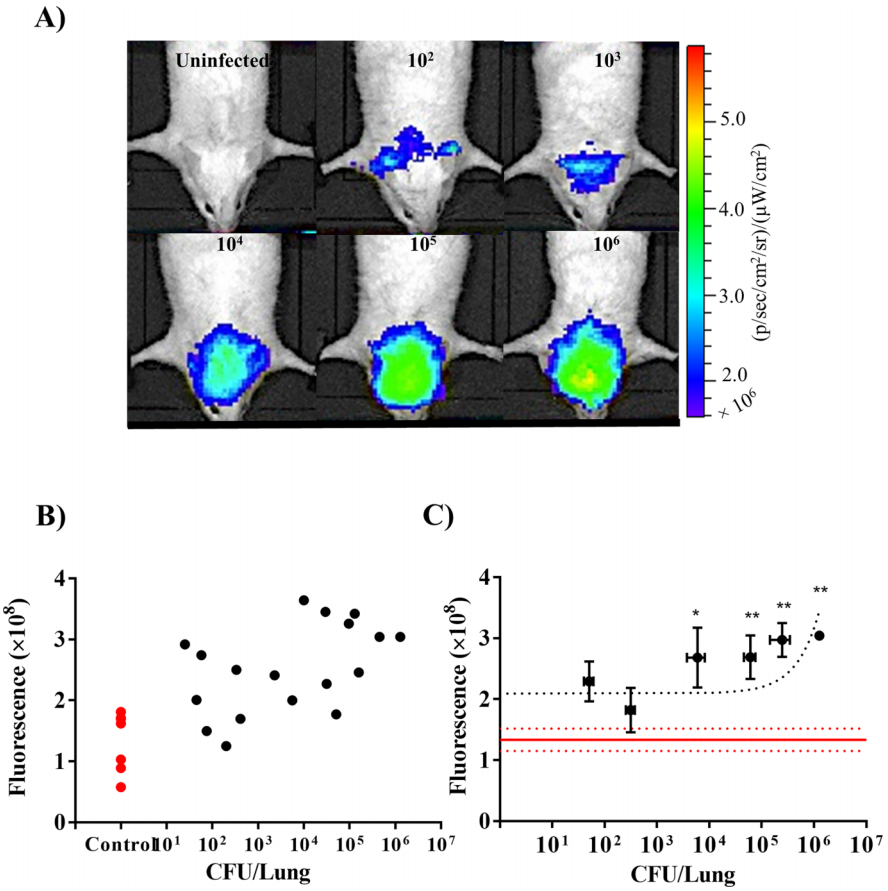

Figure 6 Whole-body imaging using IVIS epi-illumination of mice infected with 10–10^6 CFU *M. bovis* BCG strain and labeled with REF substrate CNIR800 delivered intratracheally 24 hours post-infection. (**A**) Representative images 4 hours post-administration of CNIR800. (**B**) Scatter plot of fluorescence signal (photons/sec) for each animal as compared to actual CFU obtained from lung homogenates of same animal. (**C**) Average fluorescence versus grouped CFU from lung homogenates. Vertical and horizontal error bars represent standard errors of fluorescence and CFU counts per group, respectively. The average fluorescence and standard error (0.19×10^8 p/sec/cm²/sr) for the uninfected group are represented by solid and dashed red lines, respectively. * $p < 0.05$, ** $p < 0.01$: significantly different as compared to the fluorescence in the uninfected group, calculated by Student's two-tailed *t*-test.

lysis of substrate [16]. The challenge with this background is that it has the same fluorescence spectrum as the signal and cannot be removed by spectral unmixing, which is effective for removal of tissue autofluorescence. The use of CNIR800 allows application to native strains of *Mtb* and the potential for clinical translation. Our results also demonstrate improvement of detection thresholds using REF imaging in live animals compared to both epi-illumination and trans-illumination excitation [24].

Acknowledgements This work was supported by the Bill and Melinda Gates Foundation grant no. 48523, National Science Foundation CAREER award no. CBET-1254767, and National Institute of Allergy and Infectious Diseases grant no. R01AI104960.

References

[1] Global Tuberculosis Report, World Health Organization (2015).
[2] P. Glaziou, K. Floyd, D. Weil, and M. Raviglione, Int J Tuberc Lung Dis **20**, 143–144 (2016).
[3] Y. Kong, H. Yao, H. Ren, S. Subbian, S. L. Cirillo, J. C. Sacchettini, J. Rao, and J. D. Cirillo, Proc Natl Acad Sci USA **107**, 12239–12244 (2010).
[4] F. Heuts, B. Carow, H. Wigzell, and M. E. Rottenberg, Microbes Infect **11**, 1114–1121 (2009).
[5] M. J. Hickey, T. M. Arain, R. M. Shawar, D. J. Humble, M. H. Langhorne, J. N. Morgenroth, and C. K. Stover, Antimicrob Agents Chemother **40**, 400–407 (1996).
[6] F. Nooshabadi, H.-J. Yang, J. N. Bixler, Y. Kong, J. D. Cirillo, and K. C. Maitland, PLoS One **11**, e0149932 (2016).
[7] M. Wendland and D. Bumann, FEBS Lett **521**, 105–108 (2002).
[8] C. Rang, J. E. Galen, J. B. Kaper, and L. Chao, Can J Microbiol **49**, 531–537 (2003).
[9] N. M. Coulson, M. Fulop, and R. W. Titball, Microb Pathog **16**, 305–311 (1994).
[10] P. W. Andrew and I. Roberts, J Clin Microbiol **31**, 2251–2254 (1993).
[11] T. M. Arain, A. E. Resconi, M. J. Hickey, and C. K. Stover, Antimicrob Agents Chemother **40**, 1536–1541 (1996).
[12] R. Cooksey, J. Crawford, W. Jacobs, and T. Shinnick, Antimicrob Agents Chemother **37**, 1348–1352 (1993).
[13] S. L. Davis, N. A. Be, G. Lamichhane, S. Nimmagadda, M. G. Pomper, W. R. Bishai, and S. K. Jain, PLoS One **4**, e6297 (2009).
[14] S. L. Davis, E. L. Nuermberger, P. K. Um, C. Vidal, B. Jedynak, M. G. Pomper, W. R. Bishai, and S. K. Jain, Antimicrob Agents Chemother **53**, 4879–4884 (2009).

[15] H. McShane and A. Williams, Tuberculosis **94**, 105–110 (2014).
[16] H. Xie, J. Mire, Y. Kong, M. Chang, H. A. Hassounah, C. N. Thornton, J. C. Sacchettini, J. D. Cirillo, and J. Rao, Nat Chem **4**, 802–809 (2012).
[17] Y. Kong and J. D. Cirillo, Virulence **1**, 558–562 (2010).
[18] A. R. Flores, L. M. Parsons, and M. S. Pavelka Jr, Microbiology **151**, 521–532 (2005).
[19] M. I. Voskuil, K. C. Visconti, and G. K. Schoolnik, Tuberculosis **84**, 218–227 (2004).
[20] E. Sevick-Muraca, Annu Rev Med **63**, 217–231 (2012).
[21] M. Hale, Botulinum J **2**, 168–172 (2012).
[22] M. Hale, S. Riding, and B. R. Singh, Botulinum J **1**, 431–441 (2010).
[23] V. Ntziachristos, J. Ripoll, and R. Weissleder, Opt Lett **27**, 333–335 (2002).
[24] H.-J. Yang, Y. Kong, Y. Cheng, H. Janagama, H. Hassounah, H. Xie, J. Rao, and J. D. Cirillo, J Infect Dis, DOI: 10.1093/infdis/jiw298.
[25] A. E. Foster, S. Kwon, S. Ke, A. Lu, K. Eldin, E. Sevick-Muraca, and C. M. Rooney, Appl Opt **47**, 5944–5952 (2008).
[26] R. Cohen, M. A. Stammes, I. H. de Roos, M. Stigter-van Walsum, G. W. Visser, and G. A. van Dongen, EJNMMI Res **1**, 1 (2011).
[27] M. Kijanka, F.-J. Warnders, M. El Khattabi, M. Lub-de Hooge, G. M. van Dam, V. Ntziachristos, L. de Vries, S. Oliveira, and P. M. van Bergen En Henegouwen, Eur J Nucl Med Mol Imaging **40**, 1718–1729 (2013).
[28] M. van Oosten, T. Schäfer, J. A. Gazendam, K. Ohlsen, E. Tsompanidou, M. C. de Goffau, H. J. Harmsen, L. M. Crane, E. Lim, and K. P. Francis, Nat Com **4** (2013).
[29] C. H. Heath, N. L. Deep, L. Sweeny, K. R. Zinn, and E. L. Rosenthal, Ann Surg Oncol **19**, 3879–3887 (2012).
[30] S. Gordon, S. Keshav, and M. Stein, Immunobiology **191**, 369–377 (1994).
[31] Y. Kong, A. R. Akin, K. P. Francis, N. Zhang, T. L. Troy, H. Xie, J. Rao, S. L. G. Cirillo, and J. D. Cirillo, Curr Protoc Microbiol **21**, 2C.3.1–2C.3.21 (2011).
[32] N. Mufti, Y. Kong, J. D. Cirillo, and K. C. Maitland, Biomed Opt Express **2**, 1121–1134 (2011).